Teaching electron diffraction and imaging of macromolecules

Wah Chiu, Michael F. Schmid, and B. V. Venkataram Prasad
Verna and Marrs McLean Department of Biochemistry and the W. M. Keck Center for Computational Biology, Baylor College of Medicine, Houston, Texas 77030 USA

ABSTRACT Electron microscopic analysis can be used to determine the three-dimensional structures of macromolecules at resolutions ranging between 3 and 30 Å. It differs from nuclear magnetic resonance spectroscopy or x-ray crystallography in that it allows an object's Coulomb potential functions to be determined directly from images and can be used to study relatively complex macromolecular assemblies in a crystalline or noncrystalline state. Electron imaging already has provided valuable structural information about various biological systems, including membrane proteins, protein–nucleic acid complexes, contractile and motile protein assemblies, viruses, and transport complexes for ions or macromolecules. This article, organized as a series of lectures, presents the biophysical principles of three-dimensional analysis of objects possessing different symmetries.

INTRODUCTION

Electron diffraction and imaging are biophysical techniques that involve computational analyses of electron microscopic data to determine the three-dimensional structures of macromolecules. The first significant high resolution biological structure revealed from electron imaging and diffraction was the transmembrane alpha helices in the purple membrane (Henderson and Unwin, 1975). Since then this technology has advanced steadily and the role of this technique in structural biology has gradually expanded. For example, recent studies demonstrated the feasibility of obtaining phases from images at high enough resolution to construct an atomic model of bacteriorhodopsin (Henderson et al., 1990). Electron imaging also is used to study specimens that do not form crystals large enough for x-ray diffraction studies (Chiu, 1982; Glaeser, 1982). Moreover, the three-dimensional structure determined by electron imaging can provide the critical link between the x-ray structures of individual proteins and their interactions with each other. These data are crucial to our understanding of cellular functions, as exemplified by the relationship between actin filament and actin crystal structure (Kabsch et al., 1990; Holmes et al., 1992). A number of examples of how this technique has been used to study structure–function relationships in various biological systems have been discussed in a recent review (Chiu, 1993).

This paper provides an outline of lecture materials for a course in molecular biophysics that is taught to first-year graduate students. We have taught this material for the past three years as part of a joint Houston Area Molecular Biophysics Training Program under the auspices of Baylor College of Medicine, Rice University, the University of Houston, and The University of Texas Houston Health Science Center. This paper focuses on only part of this two-semester course, which covers not only electron diffraction and imaging but also spectroscopy, nuclear magnetic resonance spectroscopy, x-ray crystallography, molecular dynamics, and protein engineering. Besides graduate students in molecular biophysics, undergraduate seniors in biochemistry and cell biology at Rice University also take this course. 35 students enrolled in this course in Spring 1992.

To make our lecture materials suitable for one- or two-hour lectures, we extracted portions of them and reorganized them for various graduate courses, such as Macromolecular Design and Analysis, Biomembranes, and Molecular Virology. These courses are taken by students from molecular and cell biology graduate programs who generally have little background in the physical and mathematical sciences. In these circumstances, the biological results of the electron diffraction and imaging techniques are emphasized, and the principles are described with graphic illustration of the concepts but without mathematical equations. The aims are to give the students a basic understanding of electron microscopic analysis, to examine the advantages and pitfalls of the technique, and to give the students a broad perspective of the structural approaches currently used to solve biological problems.

This lecture series covers five main topics, each requiring two hours for a thorough discussion. Students should have learned the mathematical concepts of complex numbers, Fourier transformation, and autocorrelation and cross-correlation functions before these lectures. Emphasis is placed on the homework problems that the students will do with the computer workstations available to them in the William M. Keck Center for Computational Biology. In this paper, we will discuss the theme of each of the topic areas, the concepts that are potentially difficult for students to grasp, supplemental illustrations that are not available in the published literature, reading assignments, and homework problems.

Address correspondence to Dr. Wah Chiu, Department of Biochemistry, Baylor College of Medicine, One Baylor Plaza, Houston, TX 77030, USA.

0006-3495/93/05/1610/16 $2.00

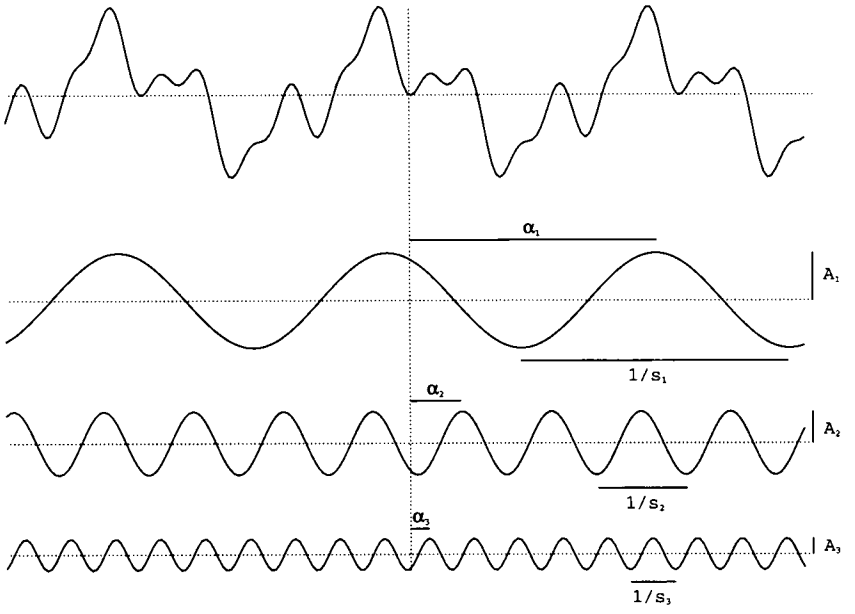

FIGURE 1 An illustration of a one-dimensional object potential function v(x) at the top of the figure which can be decomposed into three cosine waves with different frequencies (s), amplitudes (A), and phases (α) with respect to a common origin. The mathematical expression is $v(x) = \Sigma A_i(s) \cos(2\pi S_i x + \alpha_i)$. (provided by A. Avila-Sakar and V. Mootha)

LECTURE TOPIC I. BIOPHYSICAL PRINCIPLES OF ELECTRON DIFFRACTION AND IMAGING

Lecture outline

1. Description of electron microscope
2. Concept of phase problem in structure determination
3. Image phase contrast theory
4. Three-dimensional reconstruction principle
5. Methods for preservation of biological specimens
6. Radiation damage and spatial averaging
7. Data evaluation by optical diffraction
8. Digitization and sampling theorem

In this first lecture, the technique of electron microscopy is introduced. A brief description of the electron microscope and its components is given and an analogy is made to an optical microscope. In this lecture, it is important to communicate the idea that phase information is contained in the electron image data needed to determine three-dimensional structures. Many students, even those with exposure to Fourier theory, have difficulty conceptualizing how the phases enter into the reconstruction of an object's density function. An effective way of illustrating this point is to express an object's mass density function in one dimension as a sum of cosine waves where amplitude, phase, and frequency are introduced (Fig. 1).

The biophysical principles of electron diffraction and imaging can be explained in terms of diffraction physics (Cowley, 1981) or physical optics (Hoppe, 1970). The electron diffraction patterns and images can be related mathematically to an object's Coulomb potential function (also known as mass density function) by Fourier transformation (Fig. 2). This phase contrast theory is valid only when an object is thin enough and the electron energy is sufficiently high (Unwin and Henderson, 1975; Glaeser, 1982). However, there are experimental conditions under which this approximation is not adequate for extracting the optimal information from the images and the amplitude contrast has to be included for the analysis (Toyoshima and Unwin, 1988; Langmore and Smith, 1992). An important merit of the electron imaging technique is the ability to record images from which the amplitudes and phases of structure factors can be retrieved computationally. Different from x-ray crystallography, the method of retrieving phases from electron images requires a proper understanding of the Shift Theorem (Goodman, 1968; Bracewell, 1978) and the need to correct the phase reversal and amplitude modulation caused by the phase contrast transfer function $\sin \gamma(S)$ of the microscope (Thon, 1971; Amos et al., 1982; Wade, 1992).

All electron image data are two-dimensional projections of a three-dimensional object along the path of the electron beam. To obtain an object's three-dimensional Coulomb potential function, one must have image data from different angles. Such data can be obtained by different means, depending on the symmetry of the object under study. The minimal number of tilted views needed to reconstruct an object can be estimated according to geometrical considerations (Klug, 1979). Regardless of the specimen's symmetry property, the principle

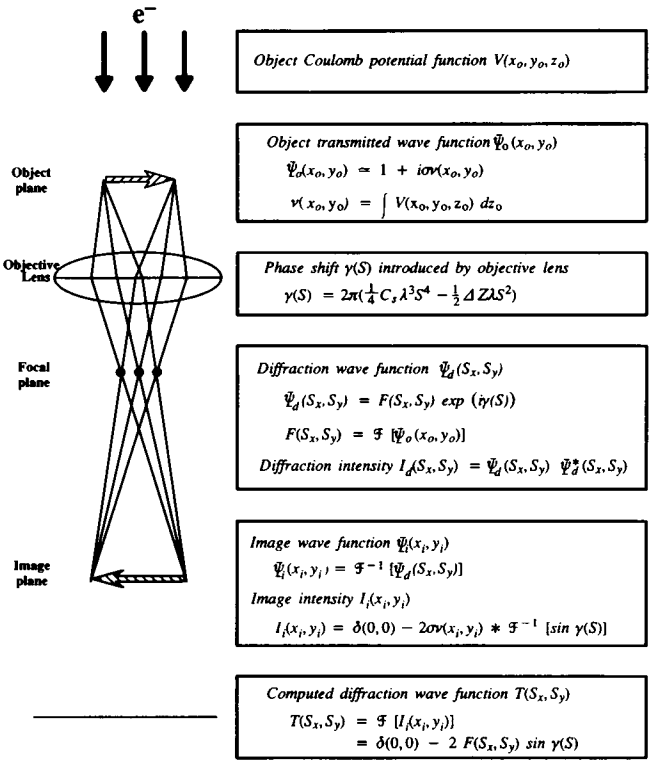

FIGURE 2 Schematic diagram of phase contrast theory (also known as weak phase approximation), which expresses the relationships among the object's Coulomb potential function, the transmitted wave function in the object plane, the diffraction wave function and intensity in the focal plane of an objective lens, the image wave function and intensity in the image plane, and the computed diffraction amplitude from digitized image intensity. This approximation is valid only if the specimen is sufficiently thin so that the transmitted wave function can be approximated in the first two terms. σ is a constant; F(S) is the structure factor which is a complex number; γ(S) is a phase shift due to the instrumental factors such as electron wavelength (λ), objective lens spherical aberration coefficient (C_s), and effective defocus value of the objective lens (ΔZ). (x, y, z) and (S_x, S_y, S_z) are the Cartesian coordinates of real and Fourier space, respectively. The subscripts (x, y, z) refer to object (o) and image (i), respectively. S is the scalar distance in Fourier space. $\mathcal{F}$ and $\mathcal{F}^{-1}$ are the symbols for forward and inverse Fourier transformation, respectively, and * is the symbol of convolution of two functions. The experimental observations in the electron microscope are the diffraction intensities (I_d) and image intensities (I_i). The aim of computer processing is to retrieve the object's Coulomb potential function $V(x_0, y_0, z_0)$. (prepared by M. J. Perez).

of three-dimensional reconstruction is the same and is based on the Central Projection Theorem (Fig. 3). This theorem can be proved easily, and its validity is based on a number of assumptions (Crowther et al., 1970). Though the operational approach of reconstructing the three-dimensional maps of the various kinds of structural architecture (i.e., crystalline, helical, icosahedral, and single-particle) are different, their underlying principles are basically the same. That is to say, they obey the same rules regarding the acquisition of sufficiently closely spaced views, the determination of orientation with respect to a common origin and phase shifting to compare and relate them, and the combination of information to produce a three-dimensional reconstruction. The special tools and techniques required for each kind of symmetry will be introduced in subsequent lectures.

Specimen preservation in a microscopic vacuum without negative stain and fixative is an important experimental concept for the technique. The glucose- (Unwin and Henderson, 1975) and ice-embedding (Taylor and Glaeser, 1974; Dubochet et al., 1988) techniques were the critical advancements that made electron imaging useful for examining biological structures in different chemical and functional states and at high resolution. Another important technical principle in electron imaging is radiation damage. Procedures carried out at low radiation doses and at low temperature reduce radiation damage to acceptable levels (Jeng and Chiu, 1984; Schmid et al., 1992). In addition, imaging efficiency at high resolutions has been improved by the recent development of computer-controlled spot-scan imaging (Downing, 1991; Brink et al., 1992). Because of the constraint of radiation damage, high-resolution images are taken with very low dose and generally have low contrast. However, the contrast can be improved by spatial

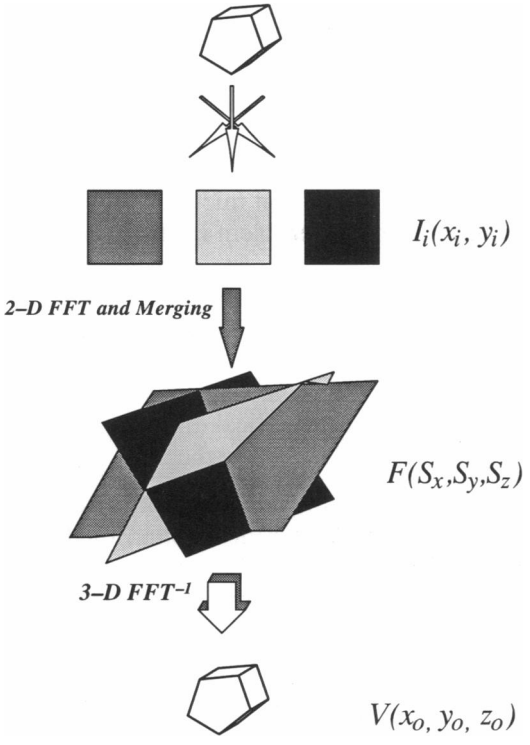

FIGURE 3 Graphical illustration of the Central Projection Theorem for three-dimensional reconstruction in electron imaging. This Theorem states that the Fourier transform of a two-dimensional projection image of an object $I_i(x_i, y_i)$ is equivalent to a section of the three-dimensional transform of that object $F(S_x, S_y, S_z)$ cutting through the center of the transform (Crowther et al., 1970). The definitions of mathematical functions are the same as those in Fig. 2. The different projections can be obtained by tilting the specimen in an electron microscope or by having the specimens lying in various orientations with respect to the electron beam (provided by Z. H. Zhou).

averaging with a computer, usually after Fourier transformation (Unwin and Henderson, 1975; Saxton and Frank, 1977; Glaeser, 1982). The method of image contrast enhancement is different for specimens with different symmetries and will be discussed in the following lecture series.

Lastly, optical diffraction is introduced as an intermediate step in evaluating the quality of image data in terms of defocus, astigmatism, and drift (Thon, 1971). Digitization of diffraction intensity and image intensity data are discussed with respect to the Sampling Theorem (Moody, 1990).

Homework problems

1. Given three cosine waves, calculate a one-dimensional density function. Introduce a variation of the amplitudes and phases in these three waves and recalculate their density function. Compare the two density functions. Manipulate the Fourier coefficients to shift the image and reverse its contrast to show its effects on the final image density.
2. Derive the electron diffraction intensity and image intensity of an object with the density function being a single cosine wave as shown in Fig. 2. The value of defocus of the image is given.
3. Plot the contrast transfer function sin $\gamma(S)$ for three different values of defocus for the given electron energy (wavelength) and spherical aberration of the objective lens.

Reading assignments

1. Glaeser (1982)—a review of the image phase contrast theory.
2. Unwin and Henderson (1984)—an introductory article on structural studies of membrane using low-dose electron microscopy.
3. Dubochet et al. (1988)—a review of specimen preparation using the ice-embedding procedure.
4. Chiu (1993)—a review of the uses of electron cryomicroscopy being different from x-ray crystallography and nuclear magnetic spectroscopy for structural studies of biological specimens.

LECTURE TOPIC II: RECONSTRUCTION OF TWO-DIMENSIONAL CRYSTALS

Lecture outline

1. Crystal formation
2. Electron diffraction
3. Low-dose images
4. Extraction of amplitudes and phases
5. Two-sided plane group determination
6. Three-dimensional reconstruction of crystalline specimens
7. Biological examples

Before this topic is discussed, it is important to introduce the concept that a two-dimensional crystal is a convolution of an asymmetric unit with a two-dimensional lattice as shown in Fig. 4. Later on, this crystal can be compared with the analogous convolutions that produce helices and icosahedral particles. Electron scattering from a two-dimensional crystal yields an intensity-weighted two-dimensional reciprocal lattice (Fig. 5).

As with x-ray crystallography, the highest resolution achieved with electron imaging has occurred in studies of highly ordered periodic arrays. The size of periodic array, or two-dimensional crystal, most amenable to electron crystallographic analysis is a few microns on edge and one cell unit thick (less than a few hundred Å). However, there is as yet limited practical experience in how to form crystals like this though their formation must obey the same thermodynamic principles as do large crystals. Three recent reviews describe crystallization methods for membrane and soluble proteins (Kornberg and Darst, 1991; Kühlbrandt, 1992; Jap et al., 1992). Once a two-dimensional crystal is formed, the best way to evaluate its quality is to study its electron diffraction pattern. The procedure used in electron crystallography for measuring electron diffraction intensity is similar to that used in x-ray crystallography (Baldwin and Henderson, 1984; Wang and Kühlbrandt, 1992). Although the integrated intensity of the diffraction spots provides an accurate measurement of the amplitudes of the crystal's structure factors, the phases are lost. As shown in Fig. 6, diffraction spots can extend beyond 3 Å from a two-dimensional crystal of streptavidin formed in the presence of a monolayer biotinylated phospholipid film (Darst et al., 1991).

Efforts to obtain images with resolutions equivalent to corresponding electron diffraction patterns have been laborious and the experimental factors have been discussed (Henderson and Glaeser, 1985; Brink and Chiu, 1991). An inherent problem is that the low dosage yields noisy images as shown in a computer-simulated example in Fig. 7. With computer processing, the structural data can be retrieved in the computed diffraction amplitudes and phases by a Fourier transformation. A filtered image with enhanced contrast of structural details can be generated from the reciprocal lattice points (Fig. 7). The computational procedure to obtain the correct phase of a crystalline specimen from a low dose image was originally described by Unwin and Henderson (1975) and has subsequently been refined by Henderson and coworkers (Baldwin et al., 1988; Henderson et al., 1990). Fig. 3 in the paper of Henderson et al. (1990) lays out the most advanced steps involved in image processing of crystals, whereas Fig. 1 of an earlier paper (Henderson et al., 1986) outlined a simpler version of the procedure. Image analysis has been made simpler and more automated (Schmid et al., 1993*a*) with recent advances in computer graphics technology. The student can develop an understanding of this part of the analysis by doing the

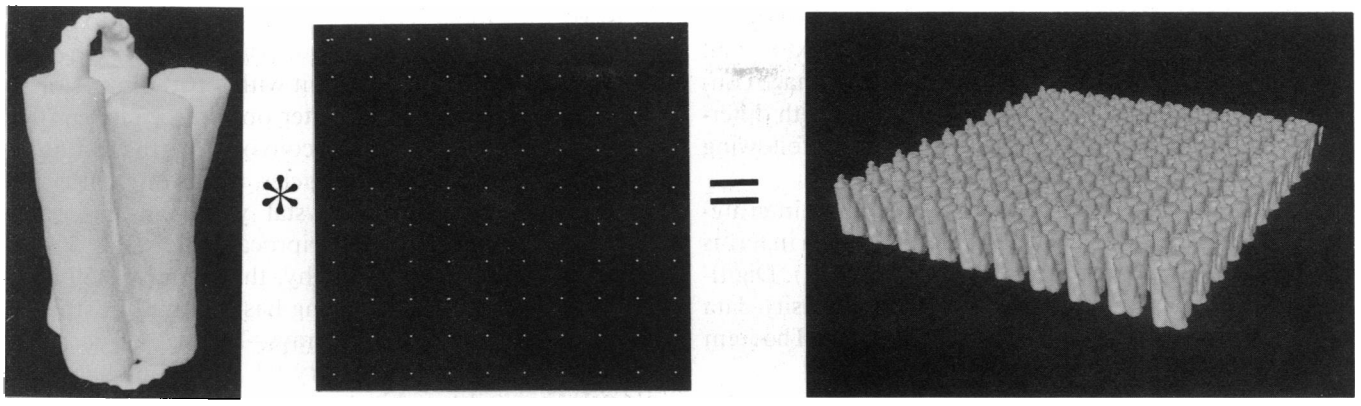

FIGURE 4 A two-dimensional crystal can be described as a convolution of an asymmetric unit and a two-dimensional lattice function. Here a four-cylinder molecular model represents the asymmetric unit. In a protein crystal, an asymmetric unit can be a single polypeptide or an integral multiple thereof.

homework on a computer workstation using the SPECTRA software developed by Schmid and co-workers (1993*a*).

The final output from image and diffraction analysis is a high-resolution projection map with phases from the image intensities and amplitudes from the electron diffraction intensities as exemplified by the projection map of glucose-embedded bacteriorhodopsin in Fig. 8. The reason that amplitudes from electron diffraction patterns are used for the reconstruction is to eliminate a tedious and not fully developed step of correcting the amplitudes from the Fourier transform of the image due to the contrast transfer function and other instrumental factors. Generally, a projection map is hard to interpret in terms of its three-dimensional structure. However, this is a special case in which the density peaks correspond to the projection of nearly parallel alpha helices across the cell membrane (Unwin and Henderson, 1975). For an unknown crystal, it is important to determine its symmetry (Holser, 1958). This can be done by examining the symmetric characteristics (e.g., systematic absence of reflections) of an electron diffraction pattern (Chiu and Hosoda, 1978). More importantly, one can also evaluate the crystallographic symmetry by evaluating the phase relationship of the symmetry-related reflections in the computed Fourier transform of the image intensity (Unwin and Henderson, 1975; Robinson et al., 1988).

The next concept to be introduced in this lecture is the experimental strategy of collecting three-dimensional image data by tilting crystals in an electron microscope. The basic crystallography of the distribution of structural factors in the third dimension of a two-dimensional crystal should be discussed. The continuity of the scattering distribution is illustrated in Fig. 9, which also shows three-dimensional data sets sampled along lattice rods from a two-dimensional crystal (Amos et al., 1982). This part is often the most difficult for students to grasp because their previous instruction in the diffraction of single three-dimensional crystals does not pre-

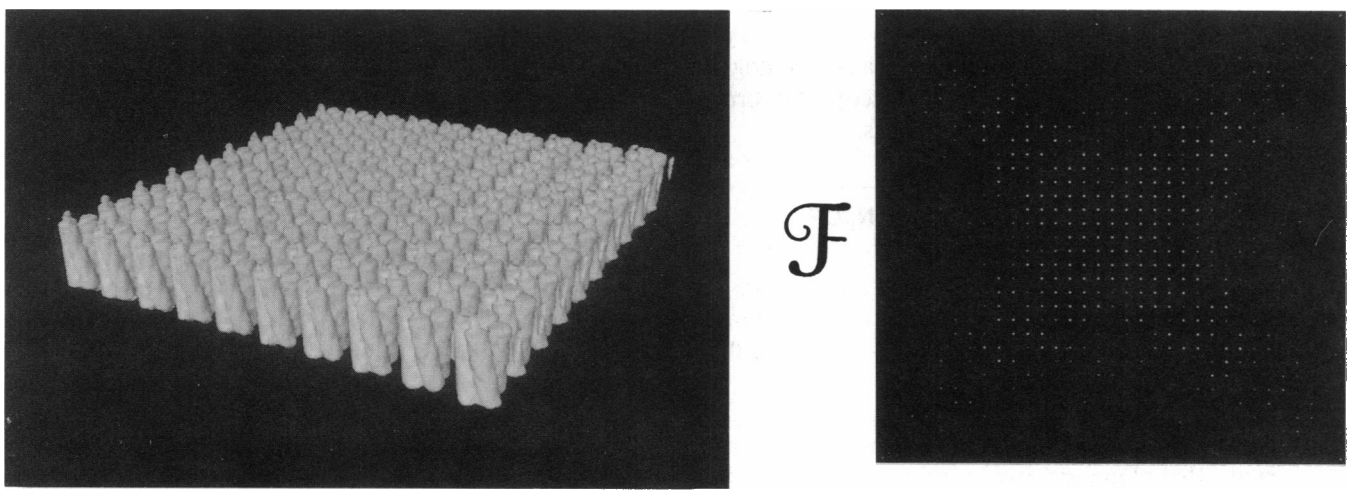

FIGURE 5 Electron diffraction pattern of a two-dimensional crystal. When an electron beam is incident onto a crystal, its diffraction pattern is a two-dimensional reciprocal lattice with its diffraction intensities weighted by the Fourier transform of the unit cell contents.

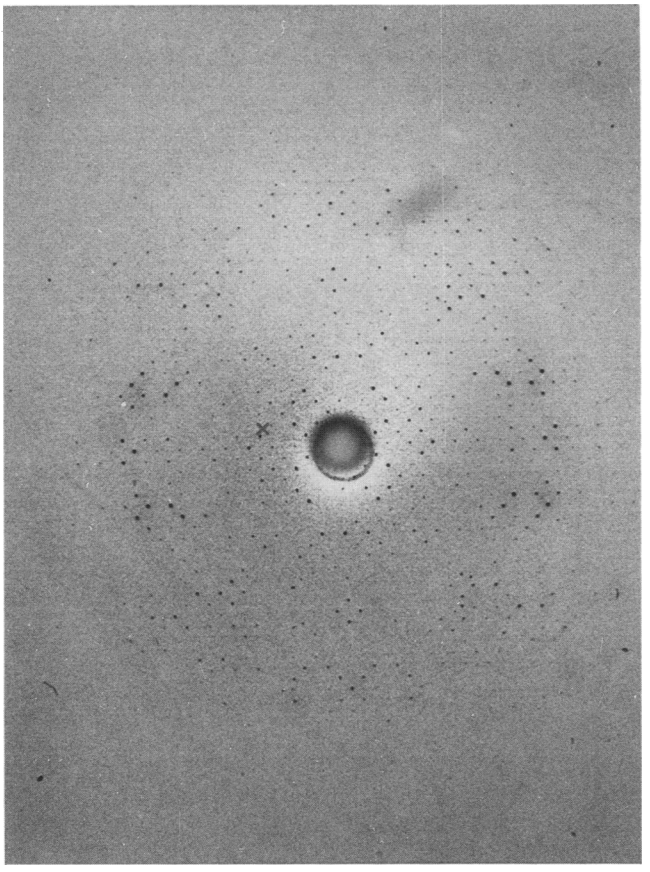

FIGURE 6 Computer-enhanced electron diffraction pattern of an ice-embedded streptavidin crystal formed in a monolayer biotinylated phospholipid film as shown by Darst and co-workers (1991). An electron diffraction pattern is formed in the focal plane of the objective lens as shown in Fig. 2 and is magnified by intermediate and projector lenses of the microscope. The two-dimensional unit cell spacing of this crystal is a = 84 Å and b = 85 Å and the diffraction spots extend beyond 3 Å resolution. (data recorded by T. L. Guan).

pare them for the concept of continuous diffraction. In the data analysis steps involved in continuous diffraction, there are several geometric parameters, including tilt angle and tilt axis, whose determination influences the accuracy of data assignments along each of the lattice rods (Shaw and Hills, 1981; Prasad et al., 1991).

There are several protein crystals that diffract at resolutions beyond 3 Å (Jeng et al., 1984; Jap et al., 1991; Kühlbrandt and Wang, 1991) that can be used as examples for discussion. Fig. 10 shows the first high-resolution image of bacteriorhodopsin in which transmembrane helices are unambiguously connected and the retinal chromophore has been located. To improve the resolution of this map, which is 3.5 Å along the x–y plane and 7 Å along the z direction, one needs to acquire better data along the z direction. Both preparing a flatter specimen (Butt et al., 1991; Glaeser, 1992) and using a computer-aided 400-kV cryomicroscope (Brink et al., 1992) can enhance the efficiency of data collection for tilted crystals.

Homework problems

1. Using SPECTRA software (Schmid et al., 1993*a*) run on a color x-window terminal workstation to display a digitized image, compute an FFT, index the diffraction pattern, correct the image distortion, select the list of structure factors with adequate statistical reliability, and calculate a projection density map.
2. Generate a three-dimensional density map from a set of structure factors. Display the map in a graphic terminal and interpret the density map.

Reading assignments

1. Henderson and Unwin (1975)—first transmembrane protein seen at a resolution of 7 Å. This was the first direct experimental observation of alpha helices in membrane protein.
2. Amos et al. (1982)—an excellent review of three-dimensional analysis of a crystalline specimen.
3. Baldwin and Henderson (1984)—gives method for determining electron diffraction intensity.
4. Henderson et al. (1990)—gives the first atomic model of protein determined by electron crystallography.
5. Stewart (1988*a*)—a review of methods used to process two-dimensional crystals of proteins.

LECTURE TOPIC III: RECONSTRUCTION OF HELICAL OBJECTS

Lecture outline

1. Definition of a helical object
2. Diffraction of a helical object
3. Helical selection rule
4. Indexing diffraction pattern
5. Three-dimensional reconstruction
6. Biological applications

Many biological specimens form helical arrays in vivo or in vitro and therefore are amenable to study by electron imaging. The data collection method for determining the three-dimensional structure of a helical object differs from that for a two-dimensional crystal. Here again, introducing the concept of an object convoluted with a sampling function allows students to see the similarities and differences between helical and crystalline objects (Fig. 11). The diffraction intensity of a helix is distributed on layer lines according to the helical selection rule in terms of the number of molecules per helical repeat as shown in a computer-simulated model (Fig. 12). Because a helical array inherently gives different views of a molecule, in principle only one image is needed for three-dimensional reconstruction, albeit at a resolution limited by the number of views afforded by the helical symmetry (DeRosier and Klug, 1968). The most critical part of the image analysis is to index the diffraction pattern and assign a helical selection rule

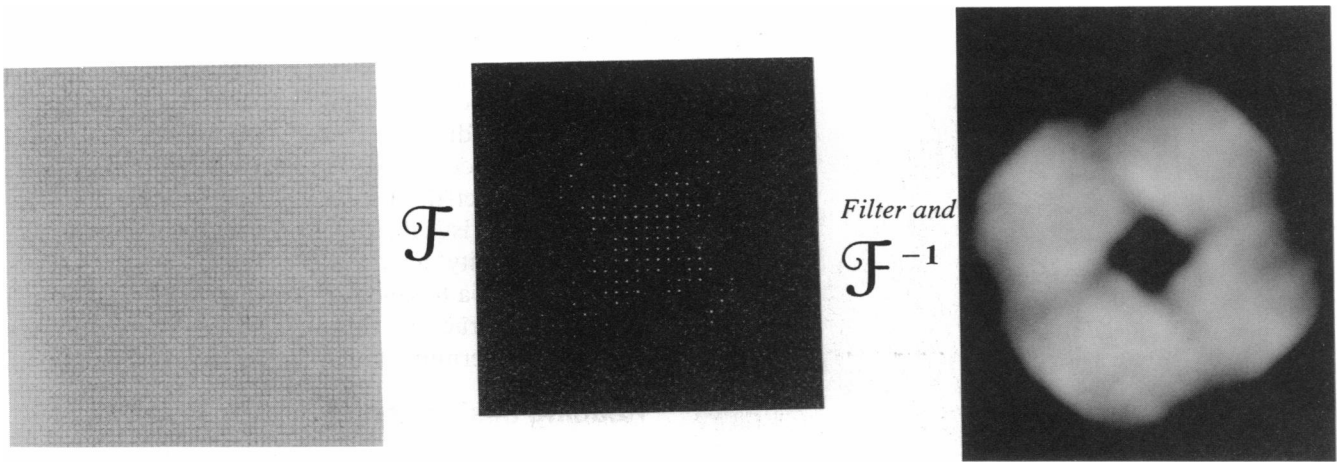

FIGURE 7 A computer-simulated low dose image of a two-dimensional crystal, its computed Fourier transform, and a computer-filtered image. Low dose can be simulated by adding white noise, in this case ranging from 0 to 4 times the highest projected density of the two-dimensional crystal shown in Fig. 4, and averaging twice this amount. Because of the low statistical definition, the contrast of the image is too low to reveal fine structural features. Extracting amplitudes and phases at the reciprocal lattice positions (see Fig. 5) is equivalent to averaging over all the unit cells using that lattice. The Fourier synthesis from these diffraction spots yields the "average" unit cell where structural features such as the four projected helices are clearly visible.

(Stewart, 1988*b*). Because of its symmetry, the diffraction pattern of a helical object is best described in terms of Bessel functions, the mathematical concept of which can be explained graphically. The steps for image analysis of a helical object, which include correction of image distortion, determination of the helical geometrical parameters, merging of different images, and reconstruction, have been outlined in Fig. 18 of Stewart (1988*b*). A

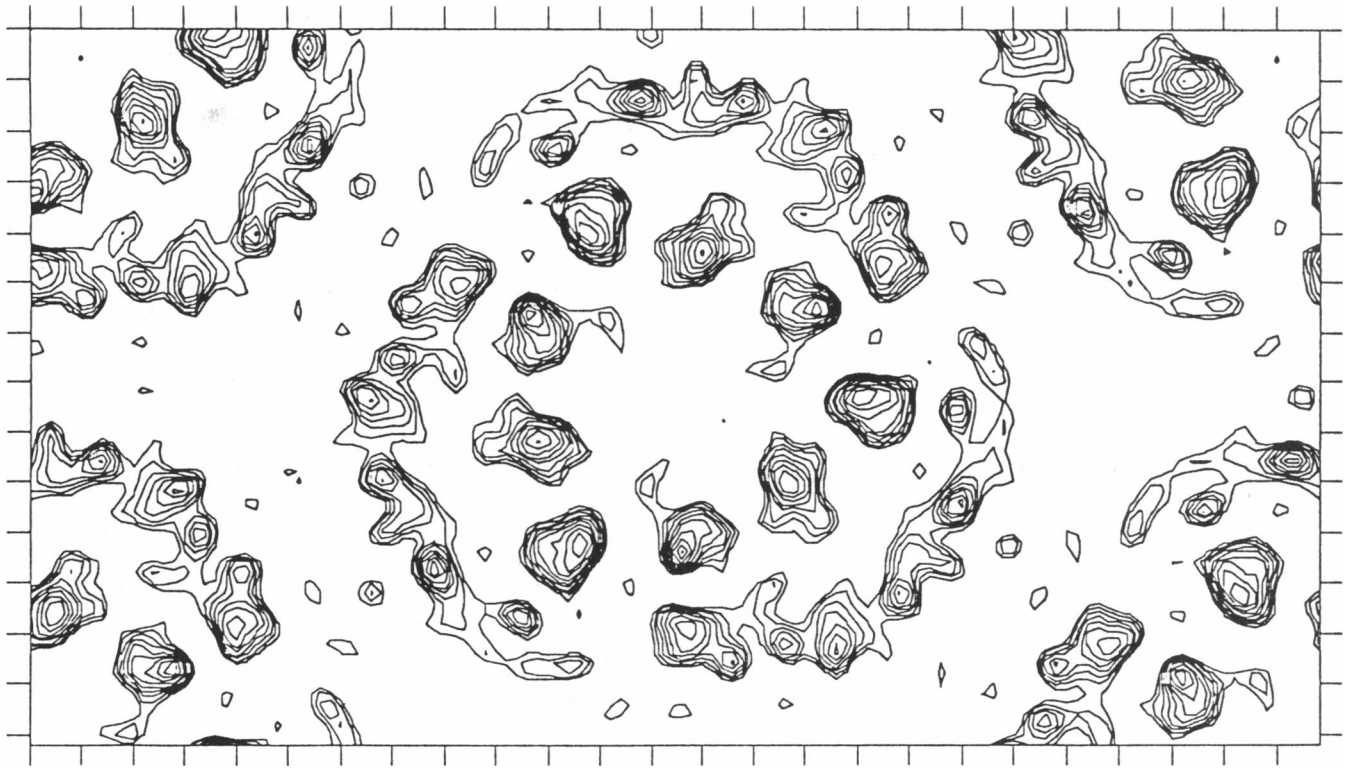

FIGURE 8 Projection density map of bacteriorhodopsin reconstructed with amplitudes from electron diffraction intensities and phases from images (Henderson et al., 1988). In principle, the amplitudes can be retrieved from the image transform but in fact they are modulated by the contrast transfer function sin $\gamma(S)$ as shown in Fig. 2. The peak densities in the map corresponds to the projection of single alpha helices in the membrane proteins. There are seven helices in each bacteriorhodopsin and three bacteriorhodopsin molecules make up one unit cell in a p3 hexagonal array of a = 62 Å and the molecular thickness of 45 Å (provided by K. H. Downing).

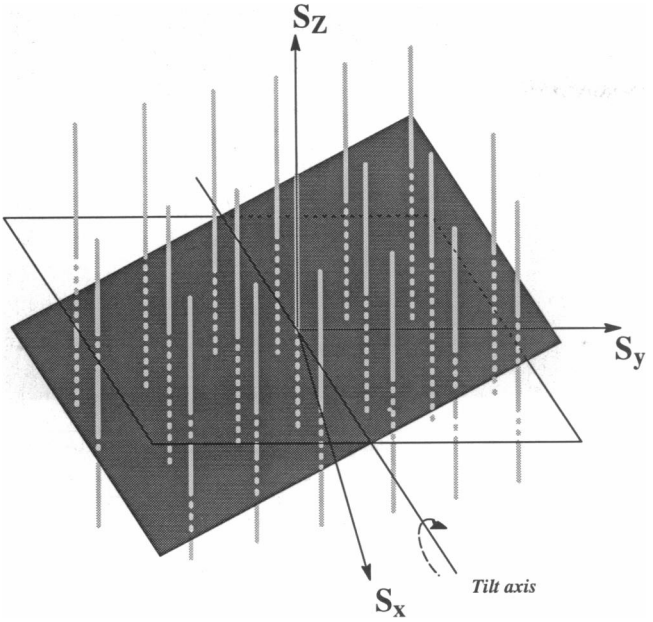

FIGURE 9 Three-dimensional Fourier space data representation of a two-dimensional crystal. The structure factors of a two-dimensional crystal are continuous along the lattice rods (Amos et al., 1982). Different sections are obtained from crystals at different tilts. The dotted points along the rods represent data behind the plane in this diagram. The sampling of the data along each lattice rod is not evenly distributed and the data must be interpolated before the three-dimensional reconstruction (provided by Z. H. Zhou).

more sophisticated scheme for retrieving high resolution data involving the correction of contrast transfer function and separation of Bessel functions has been described by Jeng and co-workers (1989). More recently, effort has been made to develop an algorithm of automating the data processing steps that one can analyze a larger set of images in order to extract the higher resolution features (Morgan and DeRosier, 1992).

Among the many helical systems that have been studied, the highest structural resolution was achieved with tobacco mosaic virus (TMV) in which the alpha helices of the coat proteins can be visualized (Fig. 13). In general, it is difficult to obtain an electron diffraction pattern from a single helical array such as single tobacco mosaic virus particle. The amplitudes and phases of this reconstruction are derived entirely from electron images. Therefore, the accuracy of its reconstruction is affected to some extent by the not fully corrected amplitudes of the structure factors (Jeng et al., 1989). There are several subcellular structures, such as bacterial flagella that are being analyzed to ~10 Å resolution (Morgan and DeRosier, 1992). Finally, the lecture can be highlighted by several interesting biological examples, such as contractile and muscle protein assembly (Milligan and Flicker, 1987; Vibert, 1992), botulism toxin tube (Schmid et al., 1993*b*), and DNA–protein complex (Chang et al., 1988; Dustin et al., 1991; Yu and Egelman 1991, 1992).

Homework problems

1. Spline fit an image of a helical object, calculate its diffraction pattern, index it, and determine its selection rule.
2. Given a set of structural factors, reconstruct the helical object three dimensionally. Display the three-dimensional map and interpret the observed features.

Reading assignments

1. DeRosier and Klug (1968)—the classic paper on three-dimensional reconstruction of electron images.
2. Stewart (1988*b*)—an excellent review of helical reconstruction.

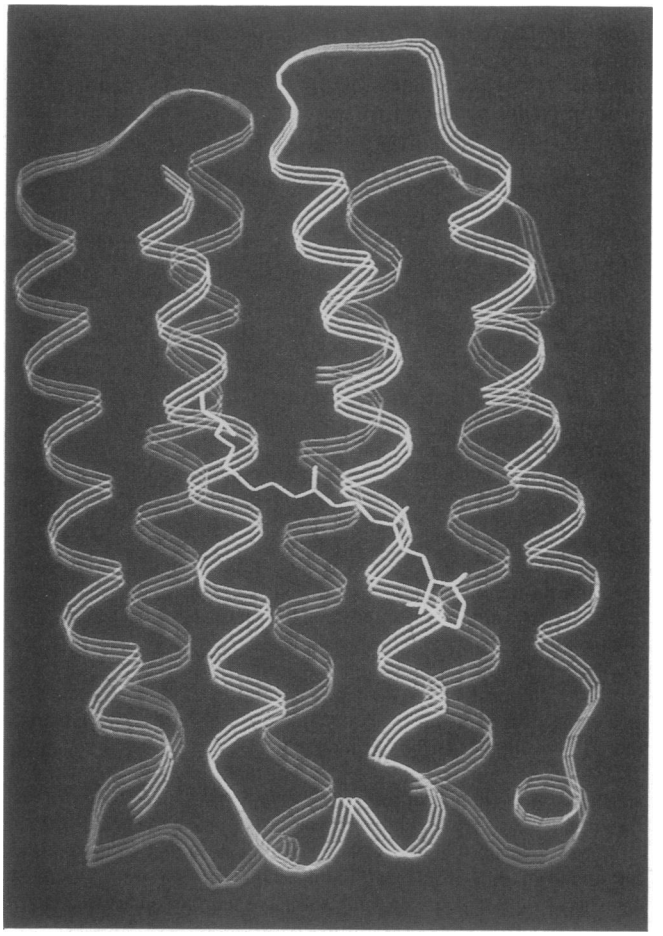

FIGURE 10 Polypeptide backbone trace of bacteriorhodopsin determined from electron crystallographic procedure (Henderson et al., 1990). The resolution was 3.5 Å in x–y plane and 7 Å in the z direction. The retinal position is well resolved in this map and its interactions with the residues in different helices have been deduced (permission of reproduction from Academic Press).

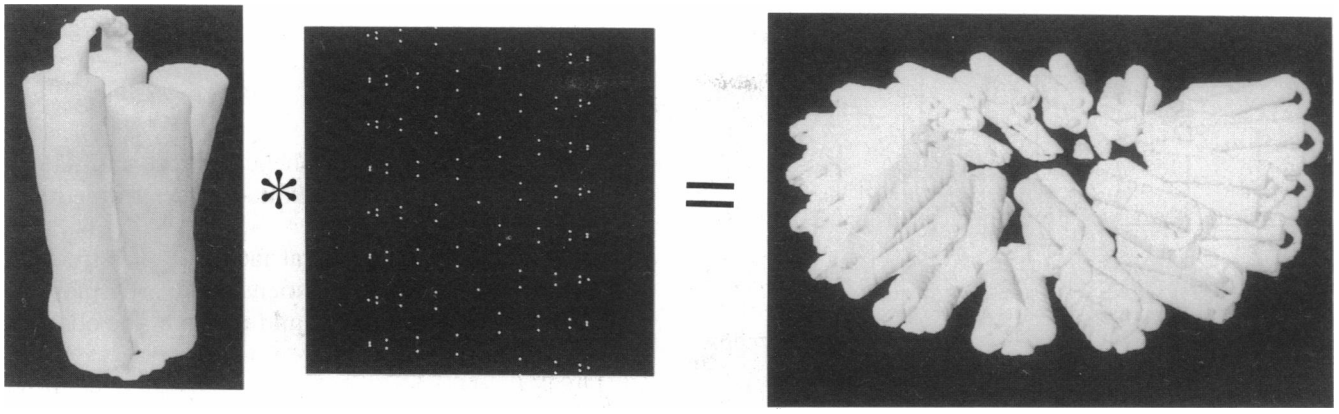

FIGURE 11 A helical array can be described as a convolution of an asymmetric unit with a helical array of points. In this example, the asymmetric unit is represented by a four-cylinder molecular model.

LECTURE TOPIC IV: RECONSTRUCTION OF ICOSAHEDRAL OBJECTS

Lecture outline

1. What is an icosahedron?
2. Triangulation number
3. Three-dimensional reconstruction scheme
4. Determining particle orientation with the "common lines" approach
5. Three-dimensional data merging in Fourier space with cylindrical coordinates
6. Biological applications

This lecture should begin with a definition of an icosahedron followed by the description of the various symmetry elements, the asymmetric unit, and the concept of triangulation, both graphically and mathematically. Excellent schematic illustrations of an icosahedron and the triangulation can be found in chapter 11 of Branden and Tooze (1991). Students usually have difficulty visualizing an icosahedron and its many subunits and symmetry axes. After describing these basic concepts the principle of quasi-equivalence is introduced (Caspar and Klug, 1962).

Now the stage is set to talk about the methodology involved in the three-dimensional reconstruction

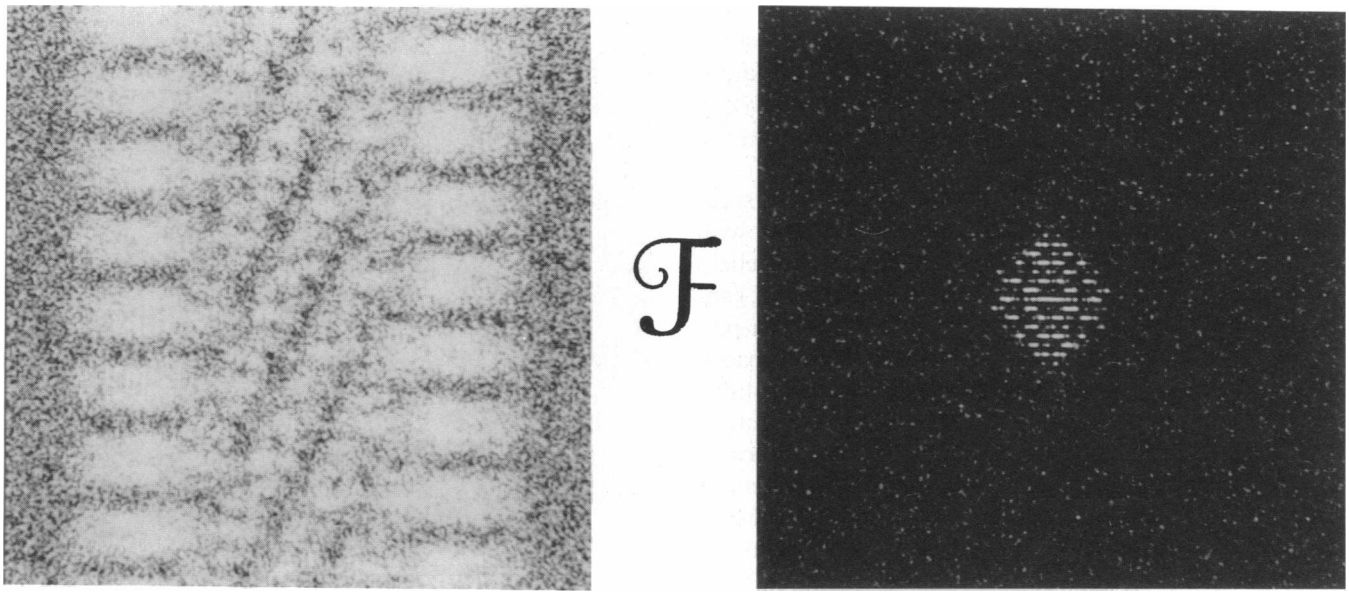

FIGURE 12 A computer-simulated low dose image of a helical array and its computed diffraction pattern. Low dose is simulated by addition of white noise in this case. Because of the translation and rotation symmetries inherent in a helical object, its diffraction intensities are localized in layer lines. The spacing between layer lines is determined according to the helical selection rule, which is described in terms of $l = tn + um$ where l is layer line number, n is the Bessel order, m is an integer, and t is the number of helical turns per u subunits.

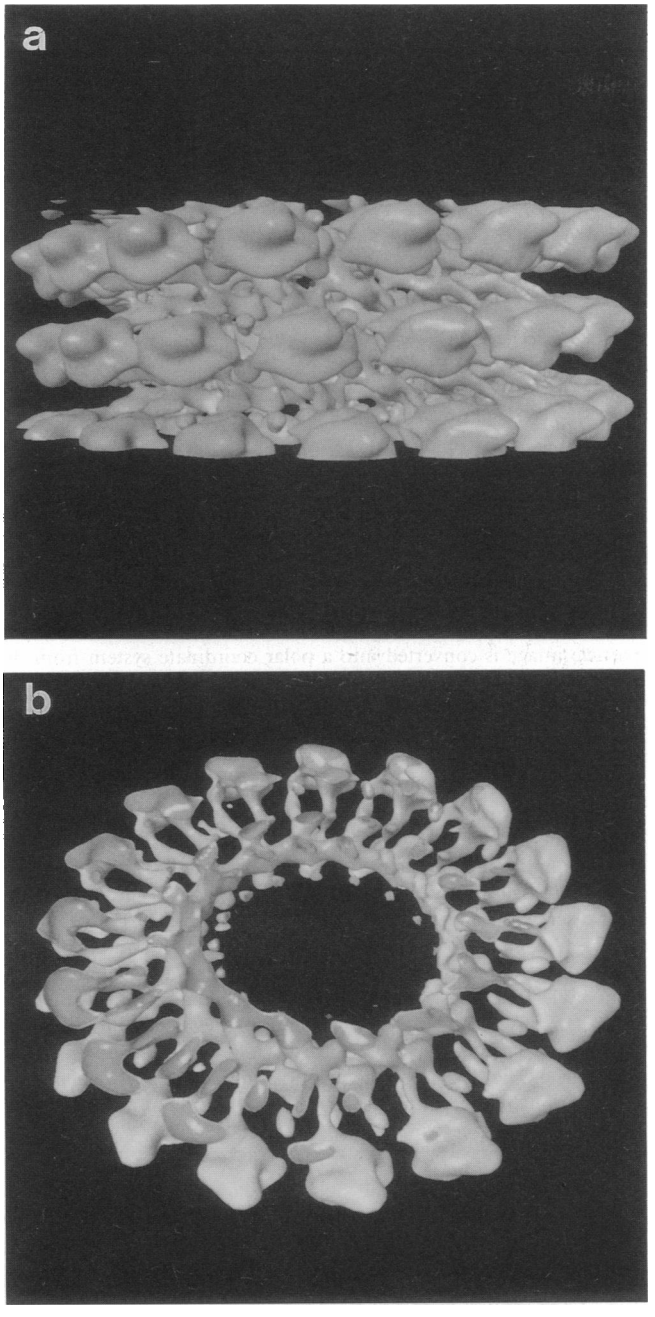

FIGURE 13 Three-dimensional surface representation of tobacco mosaic virus structure reconstructed from electron images at 9 Å resolution. (*a*) shows three helical turns of the coat protein. The helical selection rule is 49 coat proteins per helical repeat in three turns (i.e., $u = 49$, $t = 3$). (*b*) A slightly tilted view of a longitudinal section of 15 Å where the four core helix bundles in a coat protein are clearly delineated (Jeng et al., 1989).

of icosahedral particles. Fig. 14 shows a schematic outline of various steps involved in the three-dimensional reconstruction of icosahedral particles. As in the case of crystalline and helical objects, here also the three-dimensional reconstruction is premised on the Central Projection Theorem (as shown in Fig. 3). If all the different orientations of the object can be identified with respect to a common frame of reference, the three-dimensional Fourier transform of the object can be built from the two-dimensional Fourier transforms of various views. Taking advantage of the high order of symmetry present in an icosahedron, a mathematical formulation called common lines procedure was worked out for finding the orientation (Crowther, 1971). For most students the common lines concept is a difficult one to grasp. Fig. 15 is a graphical illustration of the origin of a pair of common lines in the Fourier transforms of two symmetry-related projection images. This can be generalized to explain the presence of 37 pairs of common lines in the Fourier transform of any projection image of an icosahedron. By applying the icosahedral symmetry to the Fourier transform of each projection image, 59 other identical sections in the three-dimensional Fourier transform can be generated. Thus, the data in three-dimensional Fourier space is filled in rapidly with only a few observed images. The number of particles required to carry out a reconstruction depends upon the size of the particle and the resolution. For example, a reconstruction of an icosahedral particle with a diameter of 1,000 Å to a resolution of 25 Å requires ~50 unique views. In practice, more images are used to improve the signal/noise ratio. Because of the computational convenience in applying the symmetry elements for data merging and interpolation, a spherical coordinate system (Fourier–Bes-

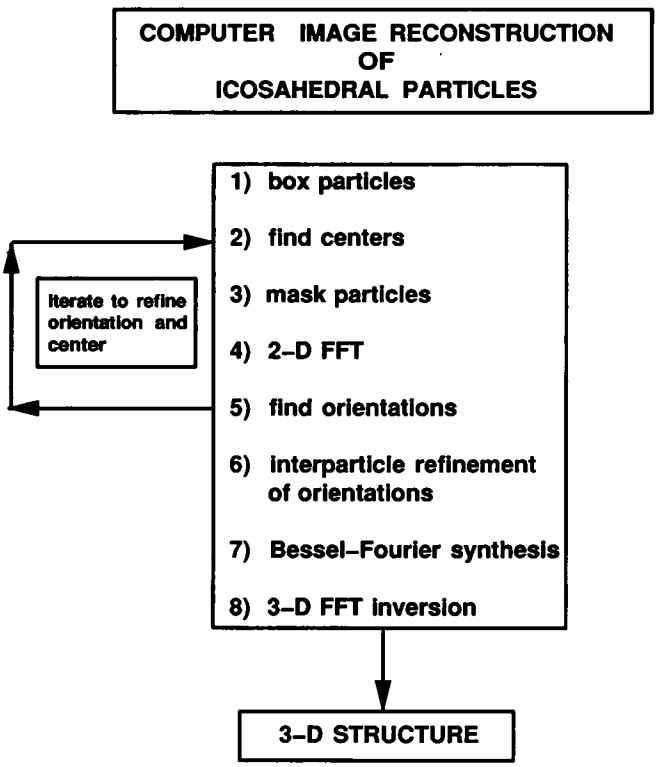

FIGURE 14 Flow chart of the various steps involved in the three-dimensional reconstruction of icosahedral particles (provided by A. L. Shaw).

sel synthesis) is used. The mathematical representations of this procedure are shown in Fig. 16. Finally, the Fourier inversion of the three-dimensional transform gives the three-dimensional structure of the icosahedral object.

Several excellent studies have related viral structures to their functions, including attachment, entry, morphogenesis, and interactions of nucleic acids and coat protein (Fuller, 1987; Schrag et al., 1989; Prasad et al., 1991; Booy et al., 1991; Wang et al., 1992; Prasad et al., 1993). Fig. 17 is an example of these studies that shows that the binding sites for Fab fragments from monoclonal antibody can be localized. Such information has provided clues about viral attachment and entry into cells (Prasad et al., 1990). Finally, the potential uses of three-dimensional electron microscopy and x-ray crystallographic analyses of large and complex viral assemblies (Stewart et al., 1991; Wang et al., 1992; Olson et al., 1992) can be discussed.

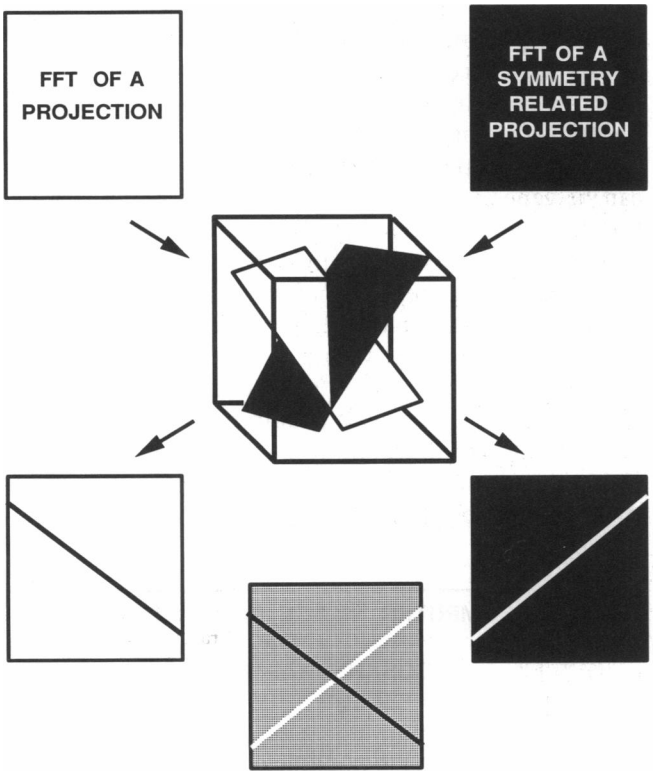

FIGURE 15 Concept of common lines procedure that is used in determining the orientation of an icosahedral particle. For simplicity, this diagram assumes an object with only one symmetry axis. By the Central Projection Theorem, there are two central sections in the Fourier transform intersecting along a line in each section. Since the two sections are identical by symmetry, the line in one section must be present in the other section. Therefore, in each section there are two lines, referred to as a pair of common lines, along which the amplitudes and phases have equivalent values. In an icosahedron, there are five-, three-, two-fold symmetry axes. These symmetry axes give rise to 37 pairs of common lines in the Fourier transform of any projection image of an icosahedral object regardless of the size and triangulation number. The angular disposition of these common lines in the Fourier transform depends on the orientation of the icosahedral particle. A major task in the reconstruction of an icosahedron is to determine the orientation parameters and refine them iteratively as shown in Fig. 14. Basically, the procedure for determining the orientation is as follows. For each possible orientation of the particle (described by a set of Euler angles), the angular disposition of all pairs of common lines is computed in advance. Then it is searched computationally along these lines to see whether the amplitudes and phases are indeed equal, and the total deviation from equality is computed for each possible particle orientation (Crowther, 1971). For the correct orientation, the deviations will usually be a minimum (provided by A. L. Shaw).

Mathematical basis of Bessel Fourier Analysis of icosahedral particle image

- *Compute Fourier transform of particles image intensity* $= T(S_r, S_\phi, S_z)$

  $$T(S_r, S_\phi, S_z) = F(S_r, S_\phi, S_z) \sin \gamma(S)$$

  $$F(S_r, S_\phi, S_z) = \sum_n G_n(S_r, S_z) \exp\left(in\left(S_\phi + \frac{\pi}{2}\right)\right) \equiv \sum_n G_n(S_r, S_z) B_n$$

- *Solve for* $G_n(S_r, S_z)$ *from a set of linear equations of particles with different orientations*

- *Compute* $g_n(r, S_z) = \int_0^\infty G_n(S_r, S_z) J_n(2\pi r S_r) 2\pi S_r dS_r$

- *Compute the Coulomb potential function by Fourier inversion*

  $$V(r, \phi, z_o) = \sum_n \int g_n(r, S_z) \exp(in\phi) \exp(2\pi i z_o S_z) dS_z$$

FIGURE 16 Mathematical and computational formulation of three-dimensional reconstruction of icosahedron particle (Crowther, 1971). To take advantage of the 5,3,2 symmetry of the particle and for computational convenience, data merging and interpolation are carried out using a cylindrical coordinate system. The Fourier transform of the particle image is converted into a polar coordinate system from the Cartesian system. The orientation of the particle allows us to determine the points where the Fourier transform of the particle's image intersects the three-dimensional Fourier transform in cylindrical coordinates (S_r, S_ϕ, S_z). The Fourier transform values of the particle are transferred into cylindrical grid. So far, all the icosahedral particle analysis has ignored the contrast transfer function $\sin \gamma(S)$ (i.e., its value is equal to 1 for all S). Icosahedral symmetry is applied to generate the values in the three-dimensional Fourier transform at all the symmetry-related positions from one single view. The operation is repeated with several particles with discrete orientations until the three-dimensional Fourier transform is filled in as much as possible. With a sufficient number of particles of discrete orientations, G_n can be solved from a set of linear equations by least-squares method. Subsequently, the g_n values are computed. In this formulation the n refers to the Bessel order and its maximum value is governed by the expected resolution and the size of the particle. The Coulomb potential function $V(r, \phi, z_0)$ in polar coordinate is finally determined by an inverse Fourier summation (prepared by M. J. Perez).

Homework problems

1. Determine the orientation of several images of viral particles.
2. Given the three-dimensional structure of a virus, describe its structural features in terms of the viral assembly principle.

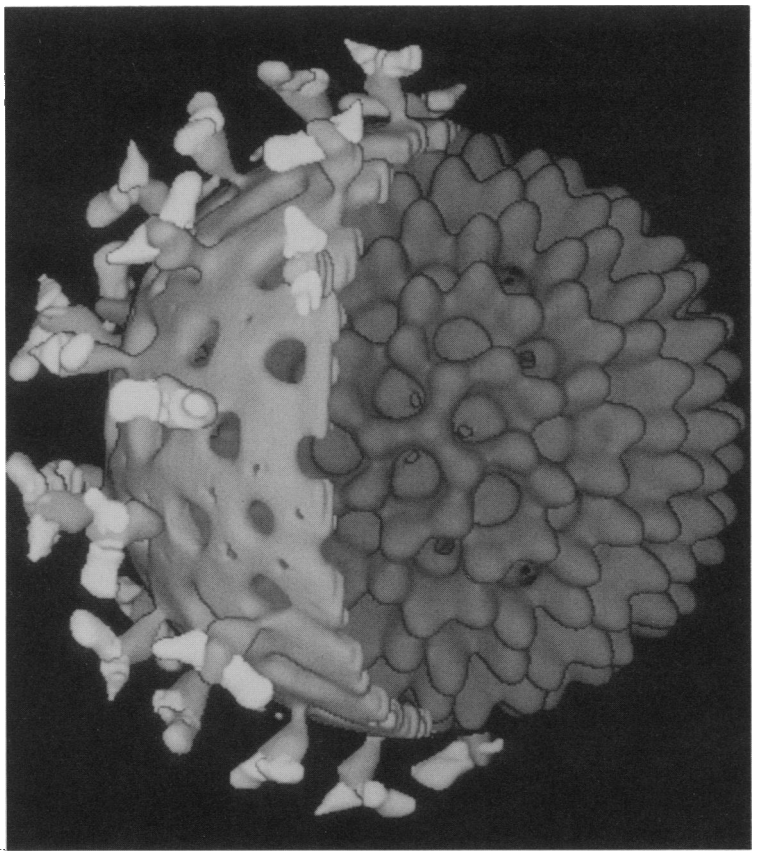

FIGURE 17 The three-dimensional map of rotavirus–Fab complex at a resolution of 40 Å. The structural analysis was carried out from electron images of randomly oriented Fab-complexed virus particles embedded in vitreous ice. The Fab molecules, shown in dark shade, are attached to all the 60 spikes. Mechanism of neutralization and the number of spike proteins were derived from this structural model (Prasad et al., 1991).

3. How many common lines in a particle with point group symmetry 432?

Reading assignments

1. Crowther (1971)—an original paper on the mathematical basis for reconstruction of icosahedral viruses.
2. Klug (1979)—a review of the early work on virus three-dimensional reconstruction.

LECTURE TOPIC V: RECONSTRUCTION OF "SINGLE-PARTICLES"

Lecture outline

1. Correlation alignment and averaging of single-particles
2. Multivariate statistical and cluster analysis
3. Random conical reconstruction
4. Evaluation of statistical reliability and interpretation of the reconstruction
5. Biological applications

Many biological macromolecules cannot be readily crystallized for a variety of reasons and therefore are not amenable to study by conventional x-ray or electron crystallographic procedures. Although electron imaging is still in its developmental stages, this technique has provided the option for obtaining the three-dimensional structures of individual macromolecules, presently at 20–50 Å resolution. Radermacher (1988) recently used a random conical approach of reconstructing single molecules and showed promising results. Fig. 5 in Radermacher's paper shows the schematic diagram of the procedure used to reconstruct single molecules in three dimensions. The best way to explain this reconstruction technique is to relate it to techniques that have been described before and to show how different views of the molecules are collected, related, and combined with each technique. However, it should be emphasized that this method differs from those discussed above because most of the data manipulation, including particle alignment, averaging, clustering, and merging, is not carried out in Fourier space. The reconstruction algorithm is called the back projection method.

In this technique, various correlation methods have been used to align molecules (van Heel and Frank, 1981; Frank, 1989; van Heel et al., 1992). This concept should be relatively easy for students to comprehend because it

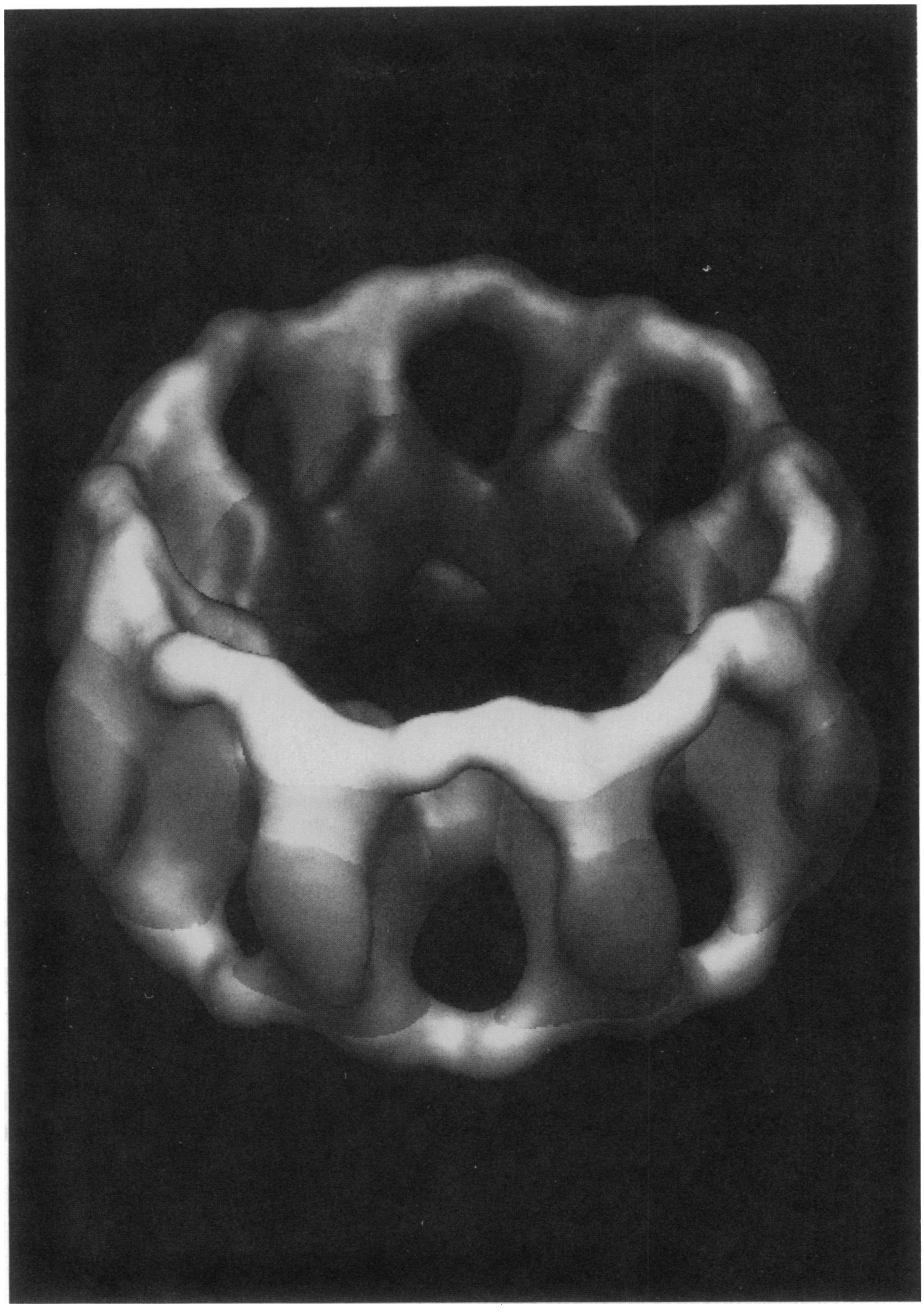

FIGURE 18 Example of an oblique view of a three-dimensional structure of nuclear pore complex purified from adult *Xenopus* oocytes and reconstructed from electron images of negatively stained single particle by averaging and multivariate statistical analysis of particles with preferred orientation. The pore has a total mass of 112×10^6 D and an overall diameter of 1,330 Å. It has four morphologically distinct subunits, that is, annular, columnar, ring-like, and lumenal. Mechanism of transport has been proposed to go through the large central channel for active transport and small peripheral channels for passive transport of small molecules and ions (provided by Hinshaw et al., 1992).

was introduced in comparisons of crystals, helices, and icosahedrons. However, the more recent mathematical tool of using eigenvector and cluster analysis to group images of individual molecules according to the feature similarity is less trivial, particularly if students have not studied matrix algebra. To make eigenvector analysis comprehensible to students, this concept can be introduced during an analysis of simple images by least-squares analysis and graphic illustration of the results. Fig. 3 in a paper by Frank (1990) gives an excellent illustration of how eigenvector analysis is used to discriminate between images on the basis of the degree of similarity in their structural features. Finally, the combined use of these computational steps gives rise to a final structure whose reliability and resolution are then analyzed (Frank and Radermacher, 1992).

Several interesting biological systems, including multipolypeptide complexes (Hinshaw et al., 1992), chan-

nels (Wagenknecht et al., 1989), and ribosome particles (Frank et al., 1991; Penczek et al., 1992), have been studied with this technique. Fig. 18 shows the single-particle reconstruction of a nuclear pore protein complex from which the transport pathway of small and large molecules has been proposed (Hinshaw et al., 1992).

Homework problem

1. Given a digitized image containing many single particles, choose a set of 25 particles, box them, filter the low-frequency components, calculate the image's correlation function for particles alignment, and derive an averaged image of aligned particles.

Reading assignments

1. Radermacher (1988)—an excellent review of the method.
2. Frank (1990)—an excellent introduction of single-particle averaging and reconstruction.

LECTURE TOPIC VI: FUTURE DEVELOPMENTS IN ELECTRON IMAGING

Lecture outline

1. Two-dimensional crystallization
2. Electron optical requirement
3. Computer-controlled data collection
4. Charged couple device camera

Except for crystalline specimens, no other types of specimens have yet been imaged close to the atomic resolution that electron imaging can potentially achieve. There have been several exciting technology developments in electron imaging: (*a*) two-dimensional crystallization of soluble and membrane proteins (Kornberg and Darst, 1991; Jap et al., 1992); (*b*) improved techniques for preparing flat specimens (Glaeser et al., 1991; Butt et al., 1991; Glaeser, 1992); (*c*) enhancements of spatial and temporal coherence by using a field emission gun and an intermediate-voltage electron microscope (Brink and Chiu, 1991; Zemlin, 1992; Zhou and Chiu, 1993); (*d*) on-line data acquisition with a charged couple device camera (Chiu et al., 1992; Koster et al., 1992); (*e*) improved data collection procedures that rely on computer control of equipment (Downing, 1991; Brink et al., 1992; Downing et al., 1992); and (*f*) novel image processing software that corrects all kinds of image distortion and enhances low-contrast signals (Frank and Radermacher, 1992; Morgan and DeRosier, 1992; Morgan et al., 1992; Saxton et al., 1992; Schmid et al., 1993*a*). This last lecture should provide an optimistic outlook for this emerging technology and show the continuing need for innovative technological advancements, which should appeal to students from physics, engineering, and the computational sciences. In addition, the exciting biological applications for these techniques should inspire cell and molecular biology students.

Reading assignments

1. Jap et al. (1992)—details crystallization methods for electron crystallography.
2. Brink, J. et al. (1992)—describes how a 400-kV electron microscope can be used for atomic imaging.
3. Downing, K. H. et al. (1992)—describes the computer-controlled operation of an electron microscope.
4. Schmid, M. F. et al. (1993*a*)—discusses image processing of two-dimensional crystals using interactive graphics.

SUMMARY

Electron imaging and diffraction for analyzing the three-dimensional structure of macromolecules is a biophysical tool that complements x-ray crystallography and nuclear magnetic resonance spectroscopy. However, the physical, mathematical, and computational bases for electron microscopic analysis differ from those of the other two techniques. This chapter offers guidance for teaching the essential principles of electron diffraction and imaging. Our experience has suggested that students best learn the principles of this technique through the hands-on experience the homework problems provide. Therefore, the availability of computer workstations with appropriate software should better facilitate teaching and learning of these biophysical techniques supplementary to lectures.

We thank Agustin Avila-Sakar, Ken Downing, Ting-Lu Guan, Jenny E. Hinshaw, Ron Milligan, Vamsi Mootha, Mary Jane Perez, Andréa Shaw, and Zhenghong Zhou for providing and preparing many of the figures shown in this manuscript. Fig. 17 is used with permission from *Annu. Rev. Biophys. Biomolec. Struct.*, Vol. 22, © by Annual Reviews Inc. The editorial assistance of Ms. Pam Powell is greatly appreciated. (Note. The SPECTRA software, homework problems, and figures are available upon request. Dr. Chiu's internet address is wah@bcm.tmc.edu.)

Our research is supported by grants GM41064, NS25877, and RR02250 from National Institutes of Health and by a grant from the W. M. Keck Foundation.

Received for publication and in final form 12 January 1993.

REFERENCES

Amos, L. A., R. Henderson, and P. N. T. Unwin. 1982. Three-dimensional structure determination by electron microscopy of 2-dimensional crystals. *Prog. Biophys. Mol. Biol.* 39:183–231.

Baldwin, J. M., and R. Henderson. 1984. Measurement and evaluation of electron diffraction patterns from 2-dimensional crystals. *Ultramicroscopy.* 14:319–335.

Baldwin, J. M., R. Henderson, E. Beckman, and F. Zemlin. 1988. Images of purple membrane at 2.8 Å resolution obtained by cryo-electron microscopy. *J. Mol. Biol.* 202:585–591.

Booy, F. P., W. W. Newcomb, B. L. Trus, J. C. Brown, T. S. Baker, and A. C. Stevens. 1991. Liquid-crystalline, phage-like packing of encapsidated DNA in herpes simplex virus. *Cell.* 64:1007–1015.

Bracewell, R. N. 1978. The Fourier Transform and Its Applications. McGraw Hill Book Co., New York.

Branden, C., and J. Tooze. 1991. Introduction to Protein Structure. Chapter 11. The Structure of Spherical Viruses. Garland Publishing, Inc., New York. 161–178.

Brink, J., and W. Chiu. 1991. Contrast analysis of cryo-images of n-paraffin recorded at 400 kV out to 2.1 Å resolution. *J. Microsc. (Oxford).* 161:279–295.

Brink, J., W. Chiu, and M. Doughtery. 1992. Computer-controlled spot-scan imaging of crotoxin complex crystals with 400 keV electrons at near atomic resolution. *Ultramicroscopy.* 46:229–240.

Butt, H. J., D. N. Wang, P. K. Hansma, and W. Kühlbrandt. 1991. Effect of surface roughness of carbon support films on high resolution electron diffraction of two-dimensional protein crystals. *Ultramicroscopy.* 36:307–318.

Caspar, D. L. D., and A. Klug. 1962. Physical principles in the construction of regular viruses. *Cold Spring Harbor Symp. Quant. Biol.* 27:1–32.

Chang, C. F., D. A. Rankert, T. W. Jeng, D. G. Morgan, M. F. Schmid, and W. Chiu. 1988. Cryo-electron microscopy of unstained, unfixed RecA-cssDNA complexes. *J. Ultrastruct. Mol. Struct. Res.* 100:166–172.

Chiu, W. 1982. High resolution electron microscopy of unstained, hydrated protein crystals. *In* Electron Microscopy of Proteins. Vol. 2. J. R. Harris, editor. Academic Press, London. 233–259.

Chiu, W. 1993. What does electron cryomicroscopy provide that x-ray crystallography and NMR spectroscopy cannot? *Annu. Rev. Biophys. Biomol. Struct.* In press.

Chiu, W., and J. Hosoda. 1978. Crystallization and preliminary electron diffraction study to 3.7 Å of DNA helix-destabilizing protein gp32*I. *J. Mol. Biol.* 122:103–107.

Chiu, W., J. Brink, T. Soejima, and M. F. Schmid. 1992. Protein electron crystallography by 400 kV cryo-microscopy. *50th Annu. Elec. Microsc. Soc. Am. Proc.* 1054–1055.

Cowley, J. M. 1981. Diffraction Physics. 2nd ed. North Holland Co., Amsterdam.

Crowther, R. A. 1971. Procedures for three-dimensional reconstruction of spherical viruses by Fourier synthesis from electron micrographs. *Philos. Trans. R. Soc. Lond. B. Biol. Sci.* 261:221–230.

Crowther, R. A., D. J. DeRosier, and A. Klug. 1970. The reconstruction of a three-dimensional structure from projections and its application to electron microscopy. *Proc. R. Soc. Lond.* 317:319–340.

Darst, S. A., M. Ahlers, P. H. Meller, E. W. Kubalek, R. Blankenburg, H. O. Ribi, H. Ringsdorf, and R. D. Kornberg. 1991. Two-dimensional crystals of streptavidin on biotinylated lipid layers and their interactions with biotinylated macromolecules. *Biophys. J.* 59:387–396.

DeRosier, D., and A. Klug. 1968. Reconstruction of 3-dimensional structures from electron micrographs. *Nature (Lond.).* 217:130–134.

Downing, K. H. 1991. Spot scan imaging in TEM. *Science (Wash. DC).* 251:53–59.

Downing, K. H., A. J. Koster, and D. Typke. 1992. Overview of computer-aided electron microscopy. *Ultramicroscopy.* 46:189–198.

Dubochet, J., M. Adrian, J.-J. Chang, J.-C. Homo, J. Lepault, A. W. McDowall, and P. Schultz. 1988. Cryo-electron microscopy of vitrified specimens. *Q. Rev. Biophys.* 21:129–228.

Dustin, I., P. Furrer, A. Stasiak, J. Dubochet, J. Langowski, and E. Egelman. 1991. Spatial visualization of DNA in solution. *J. Struct. Biol.* 107:15–21.

Frank, J. 1989. Three-dimensional imaging techniques in electron microscopy. *Biotechniques.* 7:164–173.

Frank, J. 1990. Classification of macromolecular assemblies studied as "single particles." *Q. Rev. Biophys.* 23:281–329.

Frank, J., and M. Radermacher. 1992. Three-dimensional reconstruction of single particles negatively stained or in vitreous ice. *Ultramicroscopy.* 46:241–262.

Frank, J., P. Penczek, R. Grassucci, and S. Srivastava. 1991. Three-dimensional reconstruction of the 70S *E. coli* ribosome in ice: the distribution of ribosomal RNA. *J. Cell Biol.* 115:597–605.

Fuller, S. D. 1987. The T = 4 envelope of sindbis virus is organized by interactions with a compl imentary T = 3 capsid. *Cell.* 48:923–934.

Glaeser, R. M. 1982. Electron microscopy. *Methods of Exp. Physics.* 20:391–444.

Glaeser, R. M. 1992. Specimen flatness of thin crystalline arrays: influence of the substrate. *Ultramicroscopy.* 46:33–44.

Glaeser, R. M., A. Zilker, M. Radermacher, H. E. Gaub, T. Hartmann, and W. Baumeister. 1991. Interfacial energies and surface tension forces involved in the preparation of thin, flat crystals of biological macromolecules for high resolution electron microscopy. *J. Microsc. (Oxford).* 161:21–45.

Goodman, J. W. 1968. Introduction to Fourier Optics. McGraw Hill Inc., New York.

Henderson, R., and R. M. Glaeser. 1985. Quantitative analysis of image contrast in electron micrographs of beam-sensitive crystals. *Ultramicroscopy.* 16:139–150.

Henderson, R., and P. N. T. Unwin. 1975. Three-dimensional model of purple membrane obtained by electron microscopy. *Nature (Lond.).* 257:28–32.

Henderson, R., J. M. Baldwin, K. H. Downing, J. Lepault, and F. Zemlin. 1986. Structure of purple membrane from halobacterium halobium: recording, measurement and evaluation of electron micrographs at 3.5 Å resolution. *Ultramicroscopy.* 19:147–178.

Henderson, R., J. Baldwin, T. A. Ceska, F. Zemlin, E. Beckmann, and K. H. Downing. 1990. Model for the structure of bacteriorhodopsin based on high resolution electron cryo-microscopy. *J. Mol. Biol.* 213:899–929.

Hinshaw, J. E., B. O. Carragher, and R. A. Milligan. 1992. Architecture and design of the nuclear pore complex. *Cell.* 69:1133–1141.

Holmes, K. C., M. Tirion, D. Popp, M. Lorenz, W. Kabsch, and R. A. Milligan. 1992. *In* Mechanism of myofilament sliding in muscle contraction. H. Sugi and G. H. Pollack, editors. Plenum Publishing Corp., New York. In press.

Holser, W. T. 1958. Point groups and plane groups in a two-sided plane and their subgroups. *Zeitschrift für Kristallographie,* Bd. 110:266–281.

Hoppe, W. 1970. Principles of electron structure research at atomic resolution using conventional electron microscopes for the measurement of amplitudes and phases. *Acta Crystallogr.* A26:414–426.

Jap, B. K., P. J. Walian, and K. Gehring. 1991. Structural architecture of an outer membrane channel as determined by electron crystallography. *Nature (Lond.).* 350:167–170.

Jap, B. K., M. Zulauf, T. Scheybani, A. Hefti, W. Baumeister, U. Aebia, and A. Engel. 1992. 2D crystallization: from art to science. *Ultramicroscopy.* 46:45–84.

Jeng, T. W., and W. Chiu. 1984. Quantitative assessment of radiation in a thin protein crystal. *J. Microsc. (Oxford).* 136:35–44.

Jeng, T. W., W. Chiu, F. Zemlin, and E. Zeitler. 1984. Electron imaging of crotoxin complex thin crystal at 3.5 Å. *J. Mol. Biol.* 175:93–97.

Jeng, T. W., R. A. Crowther, G. Stubbs, and W. Chiu. 1989. Visualization of alpha-helices in TMV by cryo-electron microscopy. *J. Mol. Biol.* 205:251–257.

Kabsch, W., H. G. Mannherz, D. Suck, E. F. Pai, and K. C. Holmes. 1990. Atomic Structure of the actin: DNAse I complex. *Nature (Lond.)*. 347:37–44.

Klug, A. 1979. Image analysis and reconstruction in the electron microscopy of biological macromolecules. *Chem. Scr.* 14:245–256.

Kornberg, R., and S. A. Darst. 1991. Two-dimensional crystals of proteins on lipid layers. *Curr. Opin. Struct. Biol.* 1:642–646.

Koster, A. J., H. Chen, J. W. Sedat, and D. A. Agard. 1992. Automated microscopy for electron tomography. *Ultramicroscopy.* 46:207–228.

Kühlbrandt, W. 1992. Two-dimensional crystallization of membrane proteins. *Q. Rev. Biophys.* 25:1–49.

Kühlbrandt, W., and D. N. Wang. 1991. 3-dimensional structure of plant light harvesting complex determined by electron crystallography. *Nature (Lond.)*. 350:130–134.

Langmore, J., and M. F. Smith. 1992. Quantitative energy filtered electron microscopy of biological molecules in ice. *Ultramicroscopy.* 46:349–374.

Milligan, R. A., and P. F. Flicker. 1987. Structural relationships of actin, myosin, and tropomyosin revealed by cryo-electron microscopy. *J. Cell Biol.* 105:29–39.

Moody, M. 1990. Image analysis of electron micrographs. *In* Biophysical Electron Microscopy. P. Hawkes and U. Valdrè, editors. Academic Press, San Diego. 168–170.

Morgan, D., and D. DeRosier. 1992. Processing images of helical structures: a new twist. *Ultramicroscopy.* 46:263–286.

Morgan, D. G., R. A. Grant, W. Chiu, and J. Frank. 1992. Patch averaging of electron images of gp32*I crystals with variable thickness. *J. Struct. Biol.* 108:245–256.

Olson, N. H., T. J. Smith, P. R. Kolatkar, M. A. Oliveira, R. R. Rueckert, J. M. Greve, G., R. M., and T. S. Baker. 1992. Cryoelectron microscopy of complexes of human rhinovirus with a monoclonal Fab and the viral cellular receptor. *50th Annu.* Electr. Micros. Soc. Am., Boston, San Francisco Press, San Francisco, CA. 524–525.

Penczek, P., M. Radermacher, and J. Frank. 1992. Three-dimensional reconstruction of single particles embedded in ice. *Ultramicroscopy.* 40:33–54.

Prasad, B. V. V., J. W. Burns, E. Marietta, M. K. Estes, and W. Chiu. 1990. Localization of VP4 neutralization sites in rotavirus by 3-dimensional cryo-electron microscopy. *Nature (Lond.)*. 343:476–479.

Prasad, B. V. V., L. Degn, T. W. Jeng, and W. Chiu. 1991. Estimation of allowable errors for tilt parameter determination in protein electron crystallography. *Ultramicroscopy.* 33:281–285.

Prasad, B. V. V., P. Prevelige, E. Marietta, R. Chen, D. Thomas, J. King, and W. Chiu. 1993. Three-dimensional transformation of capsids associated with genome packaging in a bacterial virus. *J. Mol. Biol.* In press.

Radermacher, M. 1988. Three-dimensional reconstruction of single particles from random and non-random tilt series. *J. Elec. Microsc. Tech.* 9:359–394.

Robinson, J., M. F. Schmid, D. Morgan, and W. Chiu. 1988. Three-dimensional structural analysis of tetanus toxin by electron crystallography. *J. Mol. Biol.* 220:367–375.

Saxton, W. O., and J. Frank. 1977. Motif detection in quantum noise-limited electron micrographs by cross-correlation. *Ultramicroscopy.* 2:219–227.

Saxton, W. O., R. Durr, and W. Baumeister. 1992. From lattice distortion to molecular distortion: characterizing and exploiting crystal deformation. *Ultramicroscopy.* 46:287–306.

Schrag, J. D., B. V. V. Prasad, F. J. Rixon, and W. Chiu. 1989. 3-dimensional structure of the HSV1 nucleocapsid. *Cell.* 56:651–660.

Schmid, M. F., J. Jakana, P. Matsudaira, and W. Chiu. 1992. Effects of radiation damage with 400 kV electrons on frozen, hydrated actin bundles. *J. Struct. Biol.* 108:62–68.

Schmid, M. F., R. Dargahi, and M. W. Tam. 1993a. SPECTRA: a system for processing electron images of crystals. *Ultramicroscopy.* In press.

Schmid, M. F., J. P. Robinson, and B. R. DasGupta. 1993b. Structure of botulism toxin channels in phospholipid vesicles. *In* Botulism, Tetanus Neurotoxins: Neurotransmission and Medical Aspects. B. R. DasGupta, editor. Plenum Publishing Corp., New York. 395–397.

Shaw, P. J., and G. J. Hills. 1981. Tilted specimen in the electron microscope: a simple specimen holder and the calculation of tilt angles for crystalline specimens. *Micron.* 12:279–282.

Stewart, M. 1988*a*. Introduction to the computer image processing of electron micrographs of two-dimensionally ordered biological structures. *J. Elec. Microsc. Tech.* 9:301–324.

Stewart, M. 1988*b*. Computer image processing of electron micrographs of biological structures with helical symmetry. *J. Elec. Microsc. Tech.* 9:325–358.

Stewart, P. L., R. M. Burnett, M. Cyrklaff, and S. D. Fuller. 1991. Image reconstruction reveals the complex molecular organization of adenovirus. *Cell.* 67:145–154.

Taylor, K. A., and R. M. Glaeser. 1974. Electron diffraction of frozen, hydrated protein crystals. *Science (Wash. DC)*. 186:1036–1037.

Thon, F. 1971. Phase contrast electron microscopy. *In* Electron Microscopy in Material Science, U. Valdré, editor. Academic Press, New York. 571–625.

Toyoshima, C., and P. N. T. Unwin. 1988. Contrast transfer for frozen, hydrated specimens: determination from pairs of defocused images. *Ultramicroscopy.* 25:279–292.

Unwin, P. N. T., and R. Henderson. 1975. Molecular structure determination of electron microscopy of unstained crystalline specimens. *J. Mol. Biol.* 94:425–440.

Unwin, P. N. T., and R. Henderson. 1984. The structure of proteins in biological membranes. *Sci. Am.* 250:78–94.

van Heel, M., and J. Frank. 1981. Use of multivariate statistics in analyzing the images of biological macromolecules. *Ultramicroscopy.* 6:187–194.

van Heel, M., M. Schatz, and E. Orlova. 1992. Correlation functions revisited. *Ultramicroscopy,* 46:307–316.

Vibert, P. 1992. Helical reconstruction of frozen, hydrated scallop myosin filaments. *J. Mol. Biol.* 223:661–671.

Wade, R. H. 1992. A brief look at imaging and contrast transfer. *Ultramicroscopy.* 46:145–156.

Wagenknecht, T., R. Grassucci, J. Frank, A. Saito, M. Inui, and S. Fleischer. 1989. Three-dimensional architecture of the calcium release channel/foot structure of sarcoplasmic recticulum. *Nature (Lond.)*. 338:167–170.

Wang, D. N., and W. Kühlbrandt. 1992. Three-dimensional electron diffraction of plant light-harvesting complex. *Biophys. J.* 61:287–297.

Wang, G., C. Porta, Z. Chen, T. Baker, and J. E. Johnson. 1992. Identification of a Fab interaction footprint site on an icosahedral virus by cryoelectron microscopy and x-ray crystallography. *Nature (Lond.)*. 355:275–278.

Yu, X., and E. H. Egelman. 1991. Image analysis reveals that *Escherichia coli* RecA protein consists of two domains. *Biophys. J.* 57:555–566.

Yu, X., and E. H. Egelman. 1992. Structural data suggest that active and inactive forms of the RecA filament are not simply interconvertible. *J. Mol. Biol.* 227:334–346.

Zemlin, F. 1992. Desired features of a cryoelectron microscope for the electron crystallography of biological material. *Ultramicroscopy.* 46:25–32.

Zhou, Z. H., and W. Chiu. 1993. Prospects of using an IVEM with a FEG for imaging macromolecules towards atomic resolution. *Ultramicroscopy.* In press.